Research Article | Vol. 8, No. 10 | 1 Oct 2018 | OPTICAL MATERIALS EXPRESS 3163

Optical Materials EXPRESS

Optical sensors based on polymeric nanofibers layers created by electrospinning

S. PONCE-ALCÁNTARA,[1] D. MARTÍN-SÁNCHEZ,[1] A. PÉREZ-MÁRQUEZ,[2] J. MAUDES,[2] N. MURILLO,[2] AND J. GARCÍA-RUPÉREZ[1,*]

[1]*Nanophotonics Technology Center, Universitat Politècnica de València, Camino de Vera s/n, 46022 Valencia, Spain*
[2]*TECNALIA, Paseo Mikeletegi 2, E-20009 Donostia-San Sebastián, Spain*
**jaigarru@ntc.upv.es*

Abstract: Porous materials have become ideal candidates for the creation of optical sensors that are able to reach extremely high sensitivities, due to both the possibility to infiltrate the target substances on them and to their large surface-to-volume ratio. In this work, we present a new alternative for the creation of porous optical sensors based on the use of polymeric nanofibers (NFs) layers fabricated by electrospinning. Polyamide 6 (PA6) NFs layers with average diameters lower than 30 nm and high porosities have been used for the creation of Fabry-Pérot optical sensing structures, which have shown an experimental sensitivity up to 1060 nm/RIU (refractive index unit). This high sensitivity, together with the low production cost and the possibility to be manufactured over large areas, make NFs-based structures a very promising candidate for the development of low-cost and high performance optical sensors.

OCIS codes: (280.4788) Optical sensing and sensors; (160.4670) Optical materials; (310.1860) Deposition and fabrication; (160.5470) Polymers; (220.2740) Geometric optical design; (050.2230) Fabry-Perot.

References and links

1. Y. Osada, D. Rossi, and E. Danilo, *Polymer Sensors and Actuators* (Springer, 2000).
2. V. S. Lin, K. Motesharei, K. P. Dancil, M. J. Sailor, and M. R. Ghadiri, "A porous silicon-based optical interferometric biosensor," Science **278**(5339), 840–843 (1997).
3. F. Vollmer and S. Arnold, "Whispering-gallery-mode biosensing: label-free detection down to single molecules," Nat. Methods **5**(7), 591–596 (2008).
4. K. Narsaiah, S. N. Jha, R. Bhardwaj, R. Sharma, and R. Kumar, "Optical biosensors for food quality and safety assurance-a review," J. Food Sci. Technol. **49**(4), 383–406 (2012).
5. S. Neethirajan, X. Weng, A. Tah, J. O. Cordero, and K. V. Ragavan, "Nano-biosensor platforms for detecting food allergens – New trends," Sens. Biosensing Res. **18**, 13–30 (2018).
6. J. Villatoro and J. Zubia, "New perspectives in optical crystal fibre sensors [invited]," Opt. Laser Technol. **78**(A), 67–75 (2016).
7. S. K. Khijwania and B. D. Gupta, "Fiber optic evanescent field absorption sensor with high sensitivity and linear dynamic range," Opt. Commun. **152**(4), 259–262 (1998).
8. C. A. Barrios, "Optical slot-waveguide based biochemical sensors," Sensors (Basel) **9**(6), 4751–4765 (2009).
9. H. Ouyang and P. M. Fauchet, "Biosensing using porous silicon optical bandgap structures," Proc. SPIE **6005**, 31–45 (2005).
10. F. A. Harraz, "Porous silicon chemical sensors and biosensors: A review," Sensor Actuat. Biol. Chem. **202**, 897–912 (2014).
11. G. A. Rodriguez, S. Hu, and S. M. Weiss, "Porous silicon ring resonator for compact, high sensitivity biosensing applications," Opt. Express **23**(6), 7111–7119 (2015).
12. C. Pacholski, "Photonic crystal sensors based on porous silicon," Sensors (Basel) **13**(4), 4694–4713 (2013).
13. S. Mariani, L. Pino, L. M. Strambini, L. Tedeschi, and G. Barillaro, "10000-fold improvement in protein detection using nanostructured porous silicon interferometric aptasensors," ACS Sens. **1**(12), 1471–1479 (2016).
14. O. Bisi, S. Ossicini, and L. Pavesi, "Porous silicon: a quantum sponge structure for silicon based optoelectronics," Surf. Sci. Rep. **38**(1–3), 6–21 (2000).
15. A. Kovacs, P. Jomnmalagadda, X. Y. Meng, and U. Mescheder, "Characterization of porous silicon based optical sensor system for biosensor applications," in *Proceedings of IEEE Sensors Conference* (IEEE, 2008), pp. 21–26.
16. Y. Zhao, G. A. Rodriguez, Y. M. Graham, T. Cao, G. Gaur, and S. M. Weiss, "Resonant photonic structures in porous silicon for biosensing," Proc. SPIE BiOS **10081**, 100810D (2017).

#331011 https://doi.org/10.1364/OME.8.003163
Journal © 2018 Received 4 May 2018; revised 26 Jun 2018; accepted 2 Jul 2018; published 20 Sep 2018

Optical Materials EXPRESS

17. R. Caroselli, D. Martín Sánchez, S. Ponce Alcántara, F. Prats Quilez, L. Torrijos Morán, and J. García-Rupérez, "Real-time and in-flow sensing using a high sensitivity porous silicon microcavity-based sensor," Sensors (Basel) **17**(12), 2813 (2017).
18. M. Iqbal, M. A. Gleeson, B. Spaugh, F. Tybor, W. G. Gunn, M. Hochberg, T. Baehr-Jones, R. C. Bailey, and L. C. Gunn, "Label-free biosensor arrays based on silicon ring resonators and high speed optical scanning instrumentation," IEEE J. Sel. Top. Quantum Electron. **16**(3), 654–661 (2010).
19. M. Balde, A. Vena, and B. Sorli, "Fabrication of porous anodic aluminium oxide layers on paper for humidity sensors," Sensor Actuat. Biol. Chem. **220**, 829–839 (2015).
20. J. Lee, K. Bae, G. Kang, M. Choi, S. Baek, D. Yoo, C. Lee, and K. Kim, "Graded-lattice AAO photonic crystal heterostructure for high Q refractive index sensing," RSC Advances **5**(88), 71770–71777 (2015).
21. S. Mohammadzadehmoghadam, Y. Dong, S. Barbhuiya, L. Guo, D. Liu, R. Umer, X. Qi, and Y. Tang, *Electrospinning: Current Status and Future Trends. Nano-size Polymers: Preparation, Properties, Applications* (Springer, 2016), Chap. 4.
22. Q. Shi, N. Vitchuli, L. Ji, J. Nowak, M. McCord, M. Bourham, and X. Zhang, "A facile approach to fabricate porous nylon 6 nanofibers using silica nanotemplate," J. Appl. Polym. Sci. **120**(1), 425–433 (2011).
23. V. S. Lin, K. Motesharei, K. P. Dancil, M. J. Sailor, and M. R. Ghadiri, "A porous silicon-based optical interferometric biosensor," Science **278**(5339), 840–843 (1997).
24. Q. Yu and X. Zhou, "Pressure sensor based on the fiber-optic extrinsic Fabry-Pérot interferometer," Photonic Sens. **1**(1), 72–83 (2011).
25. M. A. Anderson, A. Tinsley-Brown, P. Allcock, E. A. Perkins, P. Snow, M. Hollings, R. G. Smith, C. Reeves, D. J. Squirrell, S. Nicklin, and T. I. Cox, "Sensitivity of the optical properties of porous silicon layers to the refractive index of liquid in the pores," Phys. Status Solidi **197**(2), 528–533 (2003).
26. D. J. Bergman, "Dielectric-constant of a composite material – A problem in classical physics," Phys. Rep. **43**(9), 377–407 (1978).
27. J. C. Maxwell Garnett, "Colours in metal glasses and in metallic films," Philos. Trans. R. Soc. Lond. **203**(359-371), 385–420 (1904).
28. D. A. G. Bruggeman, "Calculation of various physics constants in heterogeneous substances I: dielectricity constants and conductivity of mixed bodies from isotropic substances," Ann. Phys. **416**(7), 636–664 (1935).
29. H. Looyenga, "Dielectric constants of heterogeneous mixtures," Physica **31**(3), 401–406 (1965).
30. E. K. Squire, P. A. Snow, P. S. Russell, L. T. Canham, A. J. Simons, and C. L. Reeves, "Light emission from porous silicon single and multiple cavities," J. Lumin. **80**(1–4), 125–128 (1998).
31. P. J. Reece, G. Lérondel, W. H. Zheng, and M. Gal, "Optical microcavities with subnanometer linewidths based on porous silicon," Appl. Phys. Lett. **81**(26), 4895–4897 (2002).
32. Scientific Polymer Products Inc, Refractive Index of Polymers by Index, *http://scientificpolymer.com/technical-library/refractive-index-of-polymers-by-index/*
33. P. Heikkilä and A. Harlin, "Parameter study of electrospinning of polyamide-6," Eur. Polym. J. **44**(10), 3067–3079 (2008).
34. S. Dhakate, B. Singla, M. Uppal, and R. B. Mathur, "Effect of processing parameters on morphology and thermal properties of electrospun polycarbonate nanofibers," Adv. Mater. Lett. **1**(3), 200–204 (2010).
35. T. Nitanan, P. Opanasopit, P. Akkaramongkolporn, T. Rojanarata, T. Ngawhirunpat, and P. Supaphol, "Effects of processing parameters on morphology of electrospun polystyrene nanofibers," Korean J. Chem. Eng. **29**(2), 173–181 (2012).
36. W. S. Rasband, J. Image, U. S. National Institutes of Health, Bethesda, Maryland, USA, (1997–2016), *https://imagej.nih.gov/ij/*
37. C. Huang, S. Chen, C. Lai, D. H. Reneker, H. Qiu, Y. Ye, and H. Hou, "Electrospun polymer nanofibres with small diameters," Nanotechnology **17**(6), 1558–1563 (2006).
38. R. Balili, "Transfer matrix method in nanoopticals," Int. J. Mod. Phys. Conf. Ser. **17**, 159–168 (2012).
39. W. M. Haynes, *CRC Handbook of Chemistry and Physics,* 95th Edition (CRC Press LLC, 2014–2015), Section 3, pp. 3–4.
40. J. Rheims, J. Köser, and T. Wriedt, "Refractive-index measurements in the near-IR using an Abbe refractometer," Meas. Sci. Technol. **8**(6), 601–605 (1997).
41. L. N. Acquaroli, R. Urteaga, C. L. A. Berli, and R. R. Koropecki, "Capillary filling in nanostructured porous silicon," Langmuir **27**(5), 2067–2072 (2011).

1. Introduction

Nowadays, sensors are present in a large variety of areas in our daily life, including industrial machinery and processes control, transport vehicles, building management, wearable and communications devices, environmental monitoring, sports performance, medical diagnosis or biological/chemical threats detection. Those sensors are designed to perform measurements based on mainly five transduction mechanisms: physical, chemical, optical, mechanical and electromagnetic. From those transduction mechanisms, the use of optical sensors provides important advantages compared to other technologies as for example high sensitivity, high degree of miniaturization, shorter time to result, label-free detection, requirement of very low

Optical Materials EXPRESS

volumes of sample and reagents, resistance to hazardous and harsh environments, and immunity to electromagnetic interferences [1].

Optical sensors based on the measurement of refractive index changes are widely applied to the detection of substances/analytes in many fields as clinical diagnosis, pharmaceutical and drug analysis, pollution monitoring or food control [2–6]. Most of those sensors are based on the interaction of the evanescent field of a guided mode with the surrounding media, resulting in a perturbation of the mode effective index [7,8]. However, the fact that only the lower-intensity evanescent field propagating outside the optical structure is used for sensing purposes, significantly limits the maximum achievable sensitivity. In order to overcome this limitation and to be able to use the higher-intensity optical field located inside the structure for sensing purposes, there is an increasing interest in using porous materials for the development of optical sensing structures [9–11]. Additionally, porous materials also provide an extremely higher internal surface where a huger amount of biorecognition probes can be immobilized in order to perform a selective detection of much more analytes, what is also translated into an increase of the sensitivity.

At this moment, most porous optical sensors are developed using porous silicon (PSi) substrates [12,13]. PSi can be fabricated simply, quickly and inexpensively by electrochemical etching a silicon substrate [9,14]. By properly selecting the fabrication parameters (e.g., hydrofluoric acid concentration, current density, silicon resistivity, etching time, etc.), it is possible to tune the average pore diameter, the layer porosity and the porous layer thickness. Additionally, PSi provides typical surface-to-volume ratios of the order of 500 m^2/cm^3 [14], what allows the immobilization of even more than 3 orders of magnitude more bioreceptors than for a typical solid core optical structure. Experimental sensitivities close to 330 nm/RIU (Refractive Index Unit) in the visible (VIS) and even above 1000 nm/RIU in the near infrared (NIR) ranges of the spectrum have been reported using PSi-based sensing structures [9,15–17]. These values mean an improvement in the range of one order of magnitude compared to sensitivities obtained using typical evanescent-wave sensors as for example ring resonators (maximum sensitivities around 160 nm/RIU in the NIR range of the spectrum) [18].

Other porous configuration that has gained an increasing interest during the last years is anodic aluminum oxide (AAO). As for the PSi, the fabrication process of AAO is simple and cost-effective, since it is based on a self-ordered anodization of aluminum that yields a vertically aligned and a highly ordered porous structure [19]. Sensitivities in the range of 441 nm/RIU have been reported using AAO-based porous structures measured in the VIS range of the spectrum [20].

In this work, we propose the use of polymeric nanofibers (NFs) fabricated by electrospinning for the creation of novel porous optical sensors. Electrospinning technology is currently exhibiting an exponential growth as it has attracted the attention of multiple application sectors as diverse as biomedicine (e.g., tissue engineering, cosmetics, scaffolds, drug release), environment (e.g., filtration, remediation, photocatalysis), transport and building (e.g., composites reinforcement, noise attenuation), microelectronics (e.g., batteries, supercapacitors, transistors, sensors, visualization devices) or smart textiles (e.g., wearables, smart fabrics, antibacterial, water proof, conductive, sensing textiles), among others. This rising interest is determined by the advantageous properties of the fabricated NFs-based materials, among which the most relevant ones are a high surface-to-volume ratio (of the order of 290 m^2/cm^3), a high porosity (up to 90%), an adjustable pore size, a high aspect ratio (up to 1000) without damage of their mechanical properties, a high mechanical strength, a high permeability or a great functionality versatility [21,22]. An intense research work has been carried out during the last years in the field of electrospinning fabrication, what has given rise to the development of a great variety of electrospinning process typologies as well as to the possibility of using a wide range of precursors in the fabrication process (from

Optical Materials EXPRESS

natural and synthetic polymers to emulsions or suspensions with a large variety of nanocharges as quantum dots, optical probes, nanoparticles, graphene or carbon nanotubes).

Within this context, our work has been focused on demonstrating the feasibility of using electrospinning-fabricated polymeric NFs layers as optical materials, which will then be used to create high performance optical sensors. Besides the inherent benefits of using porous materials for the development of optical sensing structures previously described (higher sensitivity and larger internal surface), the use of electrospun polymeric NFs instead of other porous materials as PSi or AAO allows having a fabrication process suitable for industrialization, since large areas can be fabricated at once with a much reduced production cost. Additionally, the sponge-like configuration of the NFs layers will allow a better filling of the sensing structure with the target substance, what will also mean an enhancement of the sensing performance.

Polyamide 6 (PA6) NFs layers fabricated by electrospinning have been experimentally studied and optimized in order to obtain a structure providing an adequate optical response and suitable to be used as optical sensor. The sensing performance of the selected PA6 NFs optical sensor has been then experimentally characterized by infiltrating the structure with acetone, obtaining a sensitivity as high as 1060 nm/RIU (Refractive Index Unit). As far as the authors know, this is the first time that a polymeric NFs layer fabricated by electrospinning is used as optical material as well as an optical sensing structure.

2. Dependence of the sensitivity with the structural properties of a porous sensing layer

Theoretical and experimental studies have shown that highly sensitive optical sensors can be developed using interferometric optical structures such as a Fabry-Pérot (FP) structures [23,24]. This type of optical sensing structure presents a reflectivity spectrum characterized by the presence of interference fringes, which are given by the constructive and destructive interferences produced by the light reflected at the interfaces between the FP layer and the upper/lower substrate.

A single layer of a porous material can be used to create a FP sensing structure, whose maxima in the reflectivity spectrum appear at wavelengths λ_m that satisfy:

$$\lambda_m = 2\, n_{eff}\, d / m, \tag{1}$$

where m is an integer, d is the layer thickness and n_{eff} is the effective refractive index of the porous layer [25]. According to Eq. (1), the reflectivity spectrum suffers a displacement if the effective refractive index of the porous layer changes; this can occur due to the modification of the refractive index of the medium filling the porous layer when a sensing measurement is carried out.

A porous medium exhibits different optical properties than its constitutive material in bulk. If the typical feature size (e.g. pore size) is much smaller than the wavelength of the incident electromagnetic field, that field will see the porous medium as a homogeneous medium having a given effective dielectric function. This effective dielectric function is dependent on the dielectric functions of both the bulk material and the filling material (e.g. air) in a ratio controlled by, amongst other parameters, the porosity.

The theory describing the dielectric function of mixed media is referred to as effective medium theory. There are several prominent effective medium models, as for example those from Bergman [26], Maxwell-Garnett [27], Bruggeman [28] and Looyenga [29]. The main difference between these models lies in how the microtopology of the pores is taken into account. In this regard, the optical response of a porous medium will change with the degree of ”connectedness” of the network and the size of the segments of material left in the medium.

Some authors suggest that the Looyenga model is more accurate for the case of high porosity layers having high pore diameters [30,31]. As it will be shown in section 3, NFs

Optical Materials EXPRESS

layers considered in this work will have a high porosity, so this will be the model used to study them. The Looyenga model is given by:

$$n_{eff}^{(2/3)} = (1-P)n_{bulk}^{(2/3)} + Pn_{void}^{(2/3)}, \quad (2)$$

where P is the porosity of the structure, n_{bulk} is the refractive index of the bulk material forming the porous structure, n_{void} is the refractive index of the medium comprising the pores and n_{eff} is the effective refractive index of the whole porous structure. This model has been used to determine the sensitivity of a porous FP sensing layer as a function of the refractive index of the bulk material forming the porous structure and of its porosity. The sensitivity parameter S has been calculated as:

$$S\left(\frac{nm}{RIU}\right) = \Delta\lambda_{peak} \Big/ \Delta n_{void}, \quad (3)$$

where $\Delta\lambda_{peak}$ is the shift of the selected peak (i.e., maximum or minimum) of the reflectance spectrum and Δn_{void} is the variation of the refractive index of the medium filling the pores of the structure. Figure 1 represents the sensitivity variation as a function of the porosity and the refractive index of the bulk material of the porous structure. For the calculations, the optical thickness ($n_{eff} \times d$) of the porous layer has been properly selected to have a maximum fringe located at 1500 nm, whose shift is measured to determine the sensitivity.

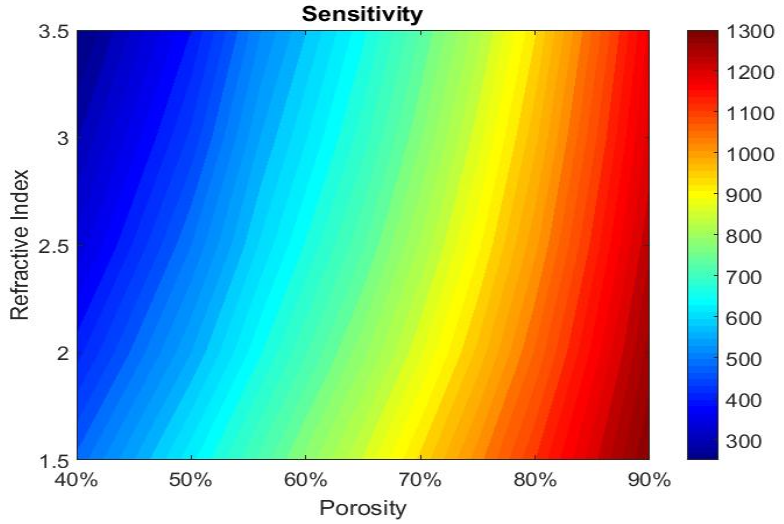

Fig. 1. Theoretical sensitivity of the porous FP sensing layer (in nm/RIU) as a function of the refractive index of the bulk material (n_{bulk} from 1.5 to 3.5) for different porosities (P from 40% to 90%).

From the results depicted in Fig. 1, it is clear that the porosity of the structure has a crucial importance on the refractive index sensitivity, since higher porosities imply that a higher volume of the structure will change its refractive index when the sensing process is carried out. However, and depending on the bulk material and the average pore diameter, higher porosities could also mean a lower structural stability of the porous layer.

Besides the porosity, the refractive index of the bulk material has also a large influence on the sensitivity of the porous FP sensing layer. In this respect, higher sensitivities can be obtained for porous FP sensing layers fabricated with lower refractive index bulk materials. Moreover, this influence of the bulk material refractive index is significantly higher if the porosity of the structure is lower. For example, a sensitivity increase of ~10% is obtained when reducing the bulk material refractive index from 3.5 to 1.5 for a layer porosity of P =

Optical Materials EXPRESS

90%; this sensitivity increase goes up to ~100% when the same variation of the bulk material refractive index is considered for a structure having a layer porosity of $P = 40\%$.

According to these the results, the use of polymeric NFs layers will allow reaching higher sensitivities, since a low refractive index bulk material will be used (typical values for polymers in the range of 1.5) and very high porosities will be typically obtained (in the range of 80-90%).

3. Fabrication of the polymeric nanofibers optical layers

3.1 Nanofibers fabrication process

One way to reduce the refractive index of the bulk material of a porous layer is by using polymeric materials as for example polycarbonate (PC), polystyrene (PS) or polyamide (PA), whose refractive indices are close to 1.5 [32]. These materials cannot be used for the creation of most typical porous substrates due to their specific fabrication process (that rely on using either silicon for PSi or aluminum for AAO). However, electrospinning process can be employed to fabricate polymeric NFs layers with adequate optical properties.

Figure 2 shows the needle-free electrospinning system used to fabricate the polymeric NFs layers studied in this work. The electrospinning solution is placed in the tank where the roller electrode, which consists in four metallic wires, is immersed. The ground collector electrode is located in the top side of the system and an antistatic substrate is placed below it to collect the flying NFs. When the electrical field applied between the roller and the ground electrodes exceeds the surface tension of the electrospinning solution, the solution jets are formed and the NFs are created during their flight from the roller to the ground electrode. The solvent in the electrospinning solution is evaporated during this flight time between the roller and the ground electrodes.

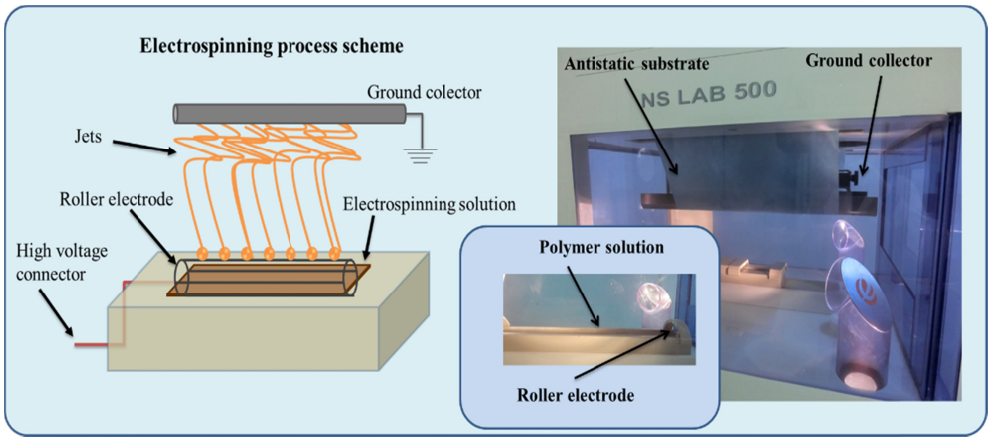

Fig. 2. Needle-free electrospinning system Nanospider 500 from El Marco used for the fabrication of the polymeric NFs layers.

The electrospinning solution used for the fabrication of the NFs layers has been prepared by dissolving a weight percentage in the range from 11 wt% to 6 wt% of PA6 pellets (Ultramid B24 N 03 purchased from BASF) in a 2:1 mixture of acetic and formic acids (purchased from Panreac Química SLU). PA6 has been selected for the creation of the NFs layers because previous results have shown that it can provide typical average diameters close to 100 nm or even lower, by properly selecting the electrospinning solution and the process parameters [33]. Other polymeric materials, as PC or PS, provide typical average diameters in the range of some hundreds of nanometers or even some microns [34,35], thus making them not suitable to achieve NFs much smaller than the light wavelength as required for the layer to behave as an optically homogeneous medium. Additionally, different salts (purchased from

Optical Materials EXPRESS

Aldrich), like tetrabutylammonium chloride (TBAC, $[CH_3(CH_2)_3]_4NCl$), potassium formate (KHCOO) or pyridine (C_5H_5N), have been independently added to the electrospinning solution in order to increase its conductivity and reduce as much as possible the diameter of the NFs. Finally, the electrospinning solution was stirred during 60 min at 80 °C.

NFs layers have been deposited over 2x2 cm^2 pieces of one side polished, boron doped, (100) monocrystalline Czochralski silicon (c-Si) wafers (purchased from Si-Mat). The wafer resistivity and thickness were 0.016 – 0.020 Ω.cm and 725 ± 15 µm, respectively. Those silicon pieces have been used to have a very flat deposition surface in order to avoid roughness interference in the NFs mesh formation. The electrospinning applied voltage has been varied from 60 kV to 75 kV in order to optimize the electrospinning process. The distance between the roller and the ground electrodes has been kept constant to 170 mm. The deposition time has been set to 20 min. The environmental conditions were a temperature of 19 ± 2 °C and a relative humidity of 40 ± 5%.

Figure 3 shows a picture of two silicon pieces without and with a deposited PA6 NFs layer.

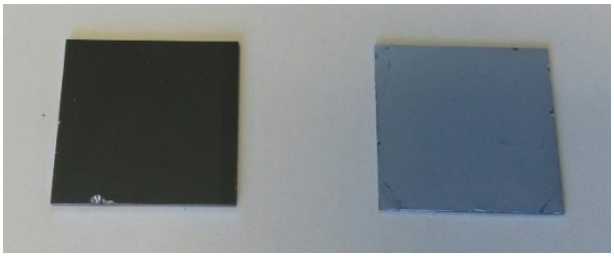

Fig. 3. (Left) Uncoated polished silicon piece. (Right) Polished silicon piece covered with a PA6 NFs layer deposited by electrospinning.

3.2 Nanofibers layer characterization and optimization

With PA6 as polymer, an iterative fabrication and characterization process has been carried out in order to optimize the electrospinning solution and the process parameters. The objective is to obtain NFs layers having a proper optical response and being suitable for their use as optical sensors. The parameters considered to optimize the electrospinning solution have been the PA6 weight percentage, the salt selected to increase the solution conductivity (TBAC, KHCOO or pyridine) and the weight percentage of that salt. The electrospinning applied voltage was adjusted to obtain the optimum NFs diameter for each solution. The characterization of the fabricated NFs layers has consisted on their physical inspection, used to determine the average diameter, the homogeneity and the defects presence of the fabricated NFs layers, and on their optical characterization, in order to determine their reflectance response.

The morphological characterization of the fabricated NFs layers has been carried out by analyzing the images obtained using a Field Emission Scanning Electron Microscope (FESEM) (Zeiss Ultra 55) and a Scanning Electron Microscope (JEOL JSM 5910-LV). Figure 4 shows some representative images of different NFs layers fabricated during the optimization study. From the obtained images, we have determined that those NFs manufactured with higher PA6 concentrations (above 10 wt%) and without any salts addition shown beads formation. By decreasing the polymer concentration, a decrease of the NFs average diameter is observed, but also an increase of beads presence is produced. After salts addition, the morphological analysis confirmed a reduction of beads, defects, irregularities or small droplets in the NFs layer, what allowed us using smaller polymer concentrations in order to reduce the NFs average diameter.

Optical Materials EXPRESS

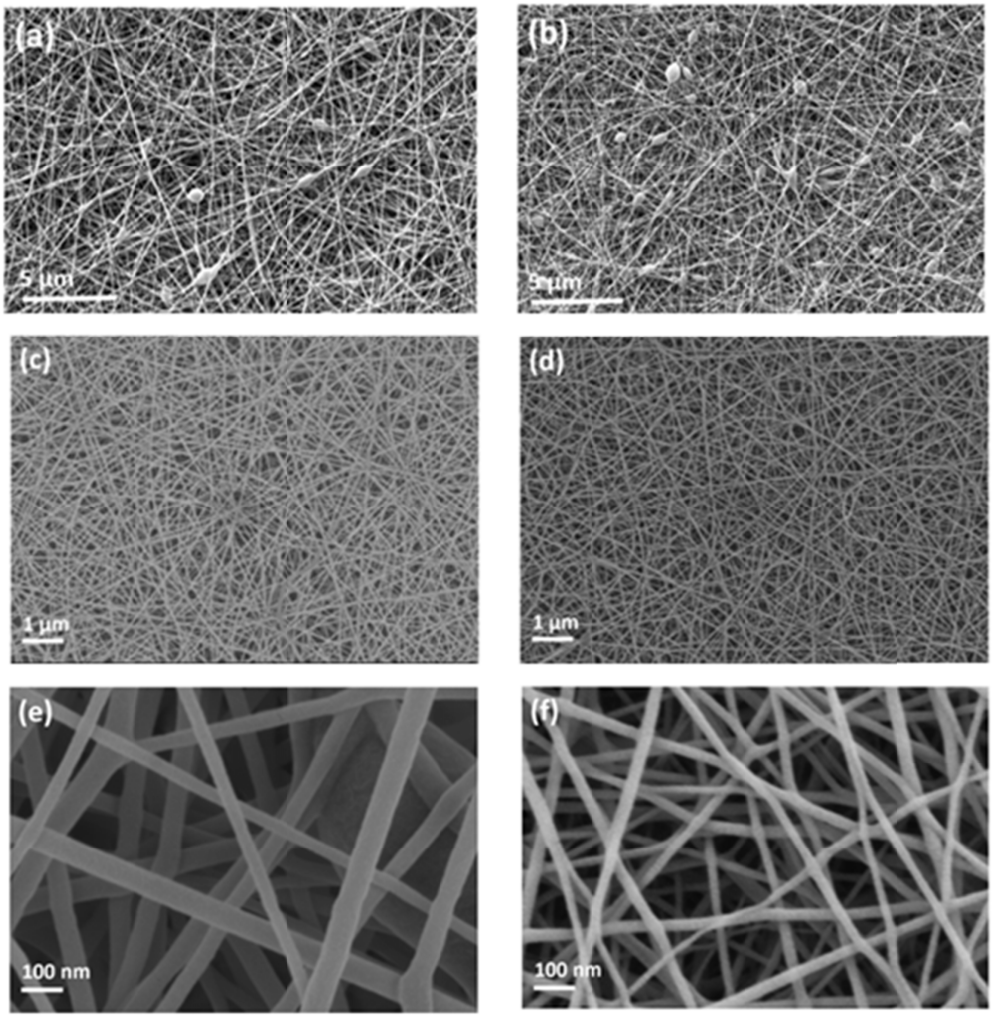

Fig. 4. Morphological characterization of representative PA6 NFs layers fabricated during the optimization steps. (a) and (b) corresponds to NFs layers with different defects, obtained with (a) 11 wt% and (b) 10 wt% of PA6, without any salt addition in the polymer solution. Images (c)-(f) shows optimized NFs layers. The electrospinning solution composition has been 9 wt% of PA6 and 1 wt% of KHCOO in (c) and (e); and 6 wt% of PA6 and 5 wt% of pyridine in (d) and (f). Three different magnifications have been used: (a) and (b) 5K (scale bar 5 µm); (c) and (d) 10K (scale bar 1 µm); (e) and (f) 100K (scale bar 100 nm).

Figure 5 shows the NFs diameters distribution respect to the percentage of PA6 and the salt content and typology in the electrospinning solution. Despite TBAC salt led to the previously commented reduction of the NFs average diameter, chopped fibers were still observed. In order to avoid these chopped fibers, KHCOO salt was added to the electrospinning solution. By reducing the PA6 concentration and increasing the KHCOO concentration, an almost exponential reduction of the NFs average diameter was obtained. However, for the PA6 7 wt% and KHCOO 5 wt% solution, an increase of the average diameter has been observed. This is due to the increment on the solution viscosity, which compensates the conductivity increase benefit of the salt addition. Therefore, a new organic salt was added to the electrospinning solution in order to further decrease the NFs average diameter. This salt was pyridine, which maintains constant the surface tension of the electrospinning solution even at small polymer concentrations [36]. By adding 5 wt% of

Optical Materials EXPRESS

pyridine to the electrospinning solution, an average diameter down to 23 ± 5.8 nm has been obtained, what is in the desired range for their application as optical layer for sensor development.

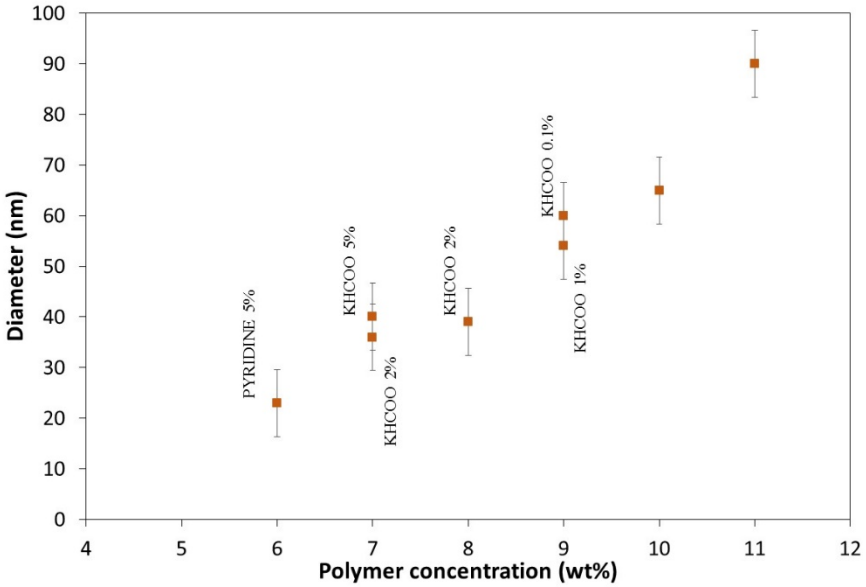

Fig. 5. NFs diameter distribution respect to the percentage of PA6 and the salt content in the electrospinning solution. The average diameter has been statistically determined with the ImageJ processing software [37].

Once the NFs samples have been morphological characterized, the quality of their optical response has been determined by measuring the specular and diffuse reflectance components using the set up schematically depicted in Fig. 6, where a 633 nm red laser beam (JDS Uniphase, model 1125) is used for the illumination. Figure 7 shows different photographs of the light reflected by the two samples without defects, previously depicted in Fig. 4(c)-(f), as well as for a bare silicon sample without NFs on it used as a reference. Figure 7(a) presents the specular reflectance of the bulk silicon sample used as support for the NFs layers. A very intense and defined reflected light spot is measured for this substrate, what is determined by the high reflectivity and the flatness of the silicon sample. When a sample having a deposited layer of higher diameter NFs is measured (see Fig. 7(b)), a lower intensity light spot is observed. In this respect, and taking as a reference the response of the polished silicon sample, the specular component of the reflected light is around 56%. Additionally, a bigger size light halo is also perceived, what corresponds to diffuse light reflection. These two effects (i.e., the reduction of the specular reflected light and the increase of the diffuse reflected light) are due to the fact that the NFs diameters are not small enough (compared to the light wavelength) to consider the layer as a homogeneous medium and the NFs will act as scattering elements. When the diameter of the deposited NFs is decreased, only a small reduction of the specular component of the reflected light compared to the bulk silicon substrate is observed and almost no diffuse reflected light is appreciated (see Fig. 7(c)). In this case, the specular component is close to 84% of the light reflected by the polished silicon sample. These two facts indicate that now the NFs are optically small enough to consider the resulting NFs layer as a homogeneous medium.

Optical Materials EXPRESS

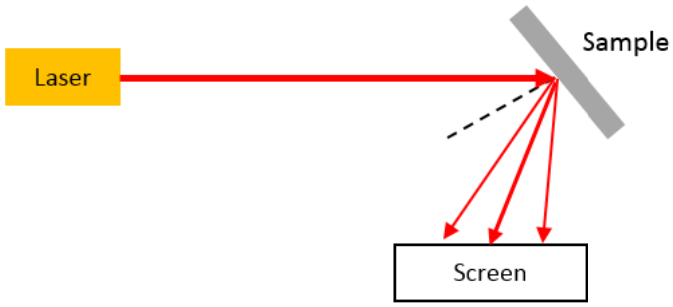

Fig. 6. Scheme of the set up used to visually determine the specular and diffuse reflectance components of the PA6 NFs layers depending on their average diameter.

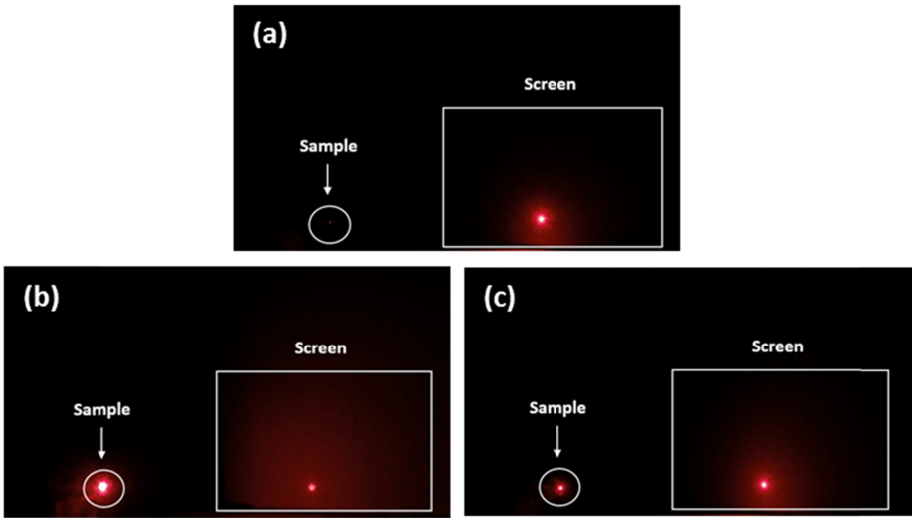

Fig. 7. Photographs of the light reflected by three different samples consisting on a polished silicon wafer (a) without any NFs layer (reference sample); (b) with a NFs layer fabricated using a 9 wt% of PA6 and 1 wt% of KHCOO; (c) with a NFs layer fabricated using a 6 wt% of PA6 and 5 wt% of pyridine.

Finally, the reflectivity spectrum of the fabricated samples has been measured using a Fourier Transform Infrared Spectroscopy (FTIR) apparatus (Bruker – VERTEX 80). Figure 8 shows the reflectivity spectra for the PA6 NFs layers without defects previously presented in Fig. 4(c)-(f). We can appreciate that a lower reflectivity is obtained for the sample having bigger NFs diameters. This reflectivity becomes even lower as the light wavelength decreases, thus confirming the influence of the NFs diameter in the reflectance response (i.e., the NFs will be optically bigger as the light wavelength decreases). Additionally, and what is even more important, the lower specular reflectance is also responsible of a low difference between the maxima and minima of the FP interference fringes appearing in the reflectivity spectrum. On the contrary, when NFs layers with smaller average diameters are deposited over the substrate, a higher reflectivity and a larger difference between the maxima and minima of the FP interference fringes in the reflectivity spectrum are observed. Therefore, small enough NFs will be required for the creation of porous layers having an appropriate optical response where the appearance of diffuse light reflection is avoided. These NFs layers will be suitable for their use as FP optical sensors.

Optical Materials EXPRESS

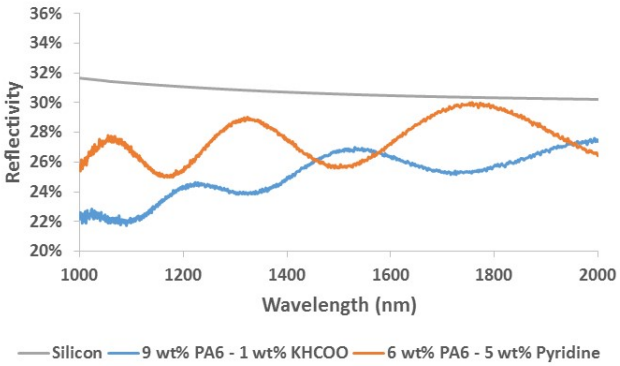

Fig. 8. FTIR specular reflectance measurement of a bulk silicon sample (gray color), a NFs layer fabricated with 9 wt% of PA6 and 1 wt% of KHCOO (blue color), and a NFs layer fabricated with 6 wt% of PA6 and 5 wt% of pyridine (orange color). FTIR measurements were performed with a resolution of 4 cm^{-1} (386 pm) and 12 scans were averaged in order to reduce the noise.

4. Experimental sensing study

According to the morphological and optical characterization previously carried out, a single layer of NFs with an average diameter below ~30 nm can optically act as FP structure. Figure 9 shows the reflectivity spectrum in the NIR spectral region of a newly fabricated NFs FP layer with 6 wt% of PA6 and 5 wt% of pyridine, with a deposition time of 20 min.

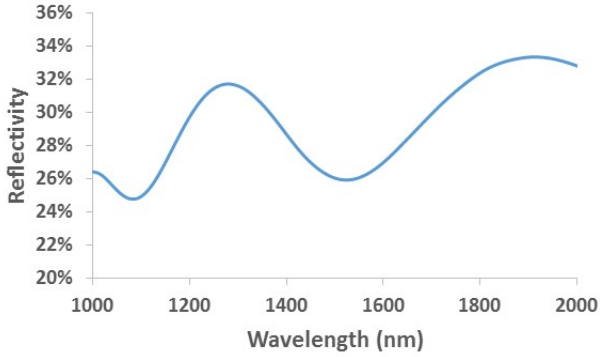

Fig. 9. Reflectivity spectrum of a NFs FP layer processed with 6 wt% of PA6 and 5 wt% of pyridine, with a deposition time of 20 minutes. A MATLAB function has been used to smooth the spectrum in order to better determine the position of the maxima/minima.

Once the PA6 NFs FP layer placed on top of a polished silicon piece has been processed, its sensing capability has been experimentally determined. In order to assess the sensing performance of the PA6 NFs FP layer as well as to confirm the influence of the porosity and the refractive index of the bulk material over the sensitivity predicted in the calculations, an additional PSi FP sensing layer has also been fabricated and experimentally characterized. The PSi layer has been fabricated by electrochemically etching a single side polished boron doped (100) oriented c-Si wafer, with a resistivity of 0.018 Ω·cm (purchased from MicroChemicals GmbH). The etching electrolyte composition was 48% hydrofluoric acid (HF) and 99% ethanol in a 1:2 volume relation. The current density used has been 34 mA/cm^2 and the etching time 150 s. In order to remove possible organic residues on the surface, the silicon wafer was cleaned with a piranha solution (volume ratio 98% sulfuric acid and 35% w/w hydrogen peroxide in a 3:1 volume ratio) at room temperature before the etching

Optical Materials EXPRESS

process. Afterwards, the wafer was rinsed with deionized water (DIW). Finally, the PSi sample was cleaned with acetone, isopropyl alcohol and DIW in order to remove organic impurities. All chemicals were of analytical grade, have been used without further purification or pre-treatment, and have been bought from Scharlab.

Table 1 shows the optical and physical properties of the two porous FP layers used in the experiments. Note that, for a better comparison, the physical thickness of the PSi layer has been appropriately selected in order to have the same optical thickness ($n_{eff} \times d$) as for the PA6 NFs layer. The Transfer Matrix Method [38] has been used to estimate the refractive index and the thickness of the porous samples from reflectivity measurements. Then, layers porosities have been calculated using the Looyenga effective medium theory, since medium-high porosity values have been obtained [29].

Table 1. Optical and physical properties of the two porous FP layers used in the experiments. Note that air-filled pores and a wavelength of 1500 nm have been considered for the calculations.

Sample	n_{bulk}	n_{eff}	Porosity	*d (nm)*	Optical thickness (nm)
PSi layer	3.50	1.86	≈60%	2495	4641
PA6 NFs layer	1.53	1.07	≈84%	4312	4614

The sensing performance of the two porous FP layers has been determined by measuring the spectral shift that is produced in the fringes pattern when a drop of acetone is deposited over the porous samples. Acetone has been used due to its low density (0.7845 mg/ml at 20°C [39]) and its notable refractive index (1.3512 at 1500 nm at 20°C [40]). Moreover, acetone needs a lower time to fill the pores in comparison with other fluids typically used in sensing measurements (e.g., methanol, ethanol or isopropanol) [41]. Reflectance measurements have been done using the same parameters than for the measurement previously shown in Fig. 9 except for the spectral range, which has been reduced to 1500-2000 nm in order to also decrease the acquisition time (to 7 seconds).

Figure 10 shows the spectral shift measured for the refractive index sensing experiments carried out using the reference PSi FP sensing layer. The spectral shift is determined from the change in the position of the minimum initially located around 1540 nm. After the deposition of a drop of acetone at t = 20 seconds, a shift of the spectrum is observed. A maximum spectral shift of 145 ± 5 nm has been measured, what determines a sensitivity of 410 ± 15 nm/RIU. Then, the spectrum is backshifted as the acetone is evaporated, until the initial spectral response is recovered (at around t = 70 seconds). Considering the porosity of this PSi sample, and according to Fig. 1, the expected theoretical sensitivity is ~620 nm/RIU. This 34% reduction in the measured experimental sensitivity compared to that theoretically calculated might be due to an incomplete filling of the pores by the acetone because of the hydraulic resistance of the liquid-PSi walls interaction [17,41].

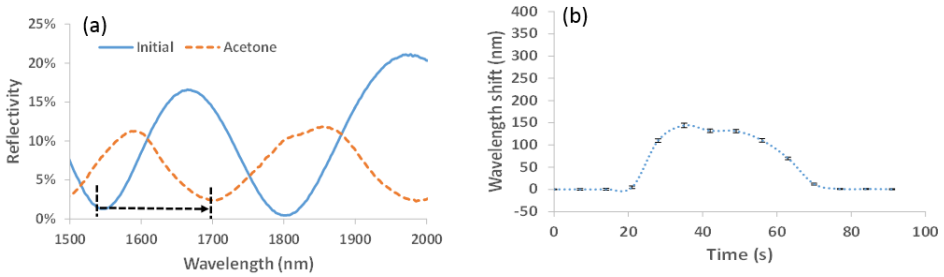

Fig. 10. (a) FTIR measured spectra for the PSi FP sensing layer having its pores filled with air (initial spectrum) and when acetone is deposited over the porous sample. (b) Temporal evolution of the spectral shift measured for the PSi FP sensing layer. Error bars for the position of the tracked spectral feature are included in the graph.

Optical Materials EXPRESS

The same acetone sensing experiment has been repeated with the optimized PA6 NFs FP layer, whose results are shown in Fig. 11. A spectral shift of 380 ± 6 nm has been measured when acetone is deposited over the porous sample, what means an experimental sensitivity of 1060 ± 18 nm/RIU. This value confirms that higher sensitivities can be obtained for porous layers created using bulk materials with a lower refractive index and with a higher porosity, as predicted in the theoretical calculations. Considering the porosity of this PA6 NFs layer, and according to the simulations results shown in Fig. 1, the expected theoretical sensitivity is ~1260 nm/RIU. Therefore, an experimental sensitivity 16% lower than that theoretically predicted has been obtained. This difference is lower than what was determined for the PSi FP sensing layer (34%), what confirms the better infiltration of the target substance due to the sponge-like configuration of the NFs layer. Moreover, the response time is also shorter than for the PSi sensing layer.

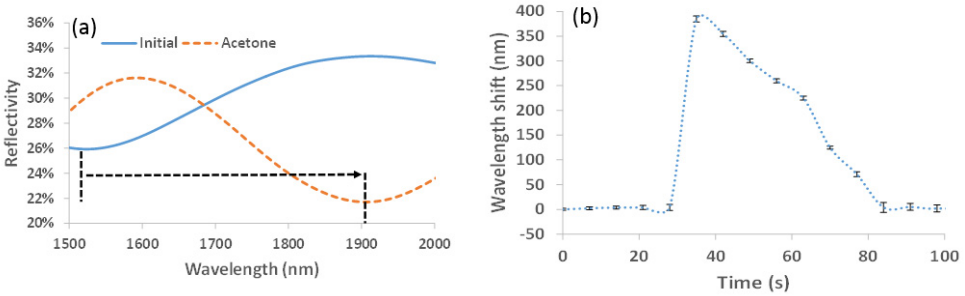

Fig. 11. (a) FTIR measured spectra for the PA6 NFs FP sensing layer being filled with air (initial spectrum) and when acetone is deposited over the sample. (b) Temporal evolution of the spectral shift measured for the PA6 NFs FP sensing layer (error bars included).

5. Conclusions

This is, to our knowledge, the first time that a NFs layer created by electrospinning is used for the development of a refractive index based optical sensor. Besides the advantages provided by other porous sensing configurations (i.e., higher sensitivities due to the possibility of infiltrating the target substances inside the structure and to the higher internal surface available to immobilize a higher number of bioreceptors), NFs sensing layers also present other advantages such as the possibility of reaching even higher sensitivities (due to the lower refractive index of the bulk polymeric materials used for their creation), a better infiltration of the target substances (due to their high porosity (see Table 1), their high pore size (see Fig. 4f), and their sponge-like configuration), and especially the possibility to fabricate them over large areas with a reduced cost and in a very simple way.

By properly adjusting the electrospinning parameters, NFs with average diameters down to 23 ± 5.8 nm have been obtained. This diameter reduction has been the key factor to achieve NFs layer with an adequate optical response, where the specular reflected component dominates over the diffuse one since the nanostructured medium is seen as an optically homogenous layer. A sensitivity of 1060 ± 18 nm/RIU has been experimentally obtained, confirming the results expected for high porosity and low bulk refractive index porous structures.

Therefore, NFs-based structures are promising candidates for the development of low-cost and high performance optical sensors.

Funding

The Spanish government (TEC2015-63838-C3-1-R-OPTONANOSENS); Basque government (KK-2017/00089-μ4F).